Nanometallurgy of Colloidal Aluminides: Soft Chemical Synthesis of $CuAl_2$ and α/β-CuAl Colloids by Co-Hydrogenolysis of $(AlCp^*)_4$ with $[CpCu(PMe_3)]$

Mirza Cokoja,[†] Harish Parala,[†] Marie-Katrin Schröter,[†] Alexander Birkner,[‡] Maurits W. E. van den Berg,[§] Wolfgang Grünert,[§] and Roland A. Fischer*,[†]

Lehrstuhl für Anorganische Chemie II - Organometallics & Materials, Ruhr-Universität Bochum, Universitätsstrasse 150, D-44780 Bochum, Germany

Received December 2, 2005. Revised Manuscript Received January 23, 2006

In this work, we present a novel soft chemical synthesis to aluminum nanoparticles based on the hydrogenolysis of the metastable organoaluminum (I) compound $(AlCp^*)_4$ (**1**) in mesitylene at 150 °C and 3 bar H_2. Aiming at the development of a general wet-chemical, nonaqueous route to M/E intermetallic nanophases (E = Al, Ga, In), we studied the co-hydrogenolysis of **1** with $[CpCu(PMe_3)]$ (**2**) as the model case aiming at Cu/Al alloyed nanoparticles. One equivalent of **1** combined with 2 equiv of **2** yields the nanocrystalline intermetallic θ-$CuAl_2$ phase ($Cu_{0.33}Al_{0.67}$), as revealed by elemental analysis, powder X-ray diffraction, transmission electron microscopy (TEM), and energy-dispersive X-ray analysis. The obtained $Cu_{0.33}Al_{0.67}$ material was also characterized by the ^{27}Al Knight Shift resonance. Alloy particles $Cu_{1-x}Al_x$ ($0.10 \leq x \leq 0.50$), typically 15 ± 5 nm (TEM) in size, are accessible as colloidal solutions by variation of the molar ratio of **1** and **2** and by the addition of poly(2,6-dimethyl-1,4-phenylene oxide) during hydrogenolysis. The ^{27}Al NMR Knight Shift resonance moves to high field starting form the value of 1639 ppm for pure nano-aluminum particles to 1486 ppm of $Cu_{0.33}Al_{0.67}$, reaching 1446 ppm for $Cu_{0.50}Al_{0.50}$, and was not detectable for Al contents below 50%. Upon oxidation (controlled exposure to the ambient), a selective oxidation of the Al component, presumably forming core−shell structured $Al_2O_3@Cu_{1-y}Al_y$ ($0.10 \leq y \leq 0.50$) particles, was studied by UV−vis spectroscopy, ^{27}Al magic-angle spinning NMR, and X-ray photoelectron spectroscopy. The Al content can be freely adjusted and lowered down to about 15 atom % ($Cu_{0.85}Al_{0.15}$) without oxidizing the Cu(0) core.

Introduction

Suitable organometallic precursors and the adaptation of colloid chemistry to nonaqueous media have pushed metal nanoparticle research beyond the limitations of both classical techniques for particle synthesis: metal salt reduction and vapor condensation.[1] But the extension of this precursor concept from transition metals to their intermetallic compounds with main group metals has not been in the focus metal colloid research so far. Aluminide nanoparticles and colloids are particularly challenging targets, however, since the discovery of quasicrystal phases in the Al (rich)−Mn system has generally revived the interest in structure and bonding of classic Hume−Rothery phases, including interest their materials properties.[2] Even certain concepts of catalyst preparation refer to aluminides. Raney-nickel is known to each freshman student in chemistry! Likewise, aqueous leaching of θ-$CuAl_2$ (khatyrkite) powder yields a highly porous copper sponge (Raney-copper) which turns into an active catalyst for methanol synthesis when promoted with ZnO and Cr_2O_3.[3] Within this context, we have previously reported in this journal on the wet-chemical, nonaqueous synthesis of nanobrass,[4] $Cu_{1-x}Zn_x$ ($0 \leq x \leq 1$), using co-pyrolysis of $ZnEt_2$ with $[Cu\{OCH(CH_3)CH_2NMe_2\}_2]$, and quite recently we have been successful in extending this study toward the development of highly efficient quasi-homogeneous, colloidal Cu/ZnO catalysts for methanol synthesis from syn-gas.[5] Consequently, we have been interested in extending our *nano*-metallurgical concept to Cu/Al phases, also aiming at a colloidal congener for the industrially important ternary $Cu/ZnO/Al_2O_3$ catalyst.[6]

The entry to a wet-chemical nanometallurgy of aluminides in general relies on a clean molecular source for bare aluminum atoms or particles in solution allowing for moderate conditions and reasonable quantities and particle concentrations. Air stable nano-Al powder, with the particle surface passivated by perfluoroalkyl carboxylic acids, has most recently been prepared by Jouet et al. using the thermal

* To whom correspondence should be addressed. E-mail: roland.fischer@ruhr-uni-bochum.de. Tel.: (+49) 234 32 24174. Fax: (+49) 234 32 14174.
[†] Lehrstuhl für Anorganische Chemie II, Ruhr-Universität Bochum.
[‡] Lehrstuhl für Physikalische Chemie 1, Ruhr-Universität Bochum.
[§] Lehrstuhl für Technische Chemie, Ruhr-Universität Bochum.

(1) (a) Dumestre, F.; Chaudret, B.; Amiens, C.; Renaud, P.; Fejes, P. *Science* **2004**, *303*, 821. (b) Botha, S. S.; Brijoux, W.; Brinkmann, R.; Feyer, M.; Hofstadt, H. W.; Kelashvili, G.; Kinge, S.; Matoussevitch, N.; Nagabhushana, K. S.; Wen, F. *Appl. Organomet. Chem.* **2004**, *18*, 566.
(2) De Laissardière, G. T.; Nguyen-Manh, D.; Mayou, D. *Prog. Mater. Sci.* **2005**, *50*, 679.
(3) Ma, L. Y.; Tran, T.; Wainwright, M. S. *Top. Catal.* **2003**, *22*, 295.
(4) Hambrock, J.; Schröter, M. K.; Birkner, A.; Wöll, C.; Fischer, R. A. *Chem. Mater.* **2003**, *15*, 4217.
(5) Schröter, M. K.; Fischer, R. A. Manuscript in preparation.
(6) Hansen, J. B. In *Handbook of Heterogeneous Catalysis*; Ertl, G., Knözinger, H., Weitkamp, J., Eds.; Wiley-VCH: New York, 1997; Vol. 4, p 1856.

10.1021/cm052667w CCC: $33.50
Published on Web 02/28/2006

decomposition of $[H_3Al(NMe_3)]$ with $[Ti(O^iPr)_4]$ as the catalyst for the alane decomposition.[7] The chemical vapor deposition of aluminum thin films by the thermal decomposition of R_3Al at temperatures typically above 300 °C is well-established. Some work has been done investigating the thermal decomposition of R_2AlH (R = H, Me, Et, ^{i}Bu) in coordinating solvents such as ethers or tertiary amines at temperatures above 200 °C.[8] Aluminide powder materials, such as NiAl[9] and PtAl,[10] were obtained by co-hydrogenolysis of $AlEt_3$ with $[Ni(cod)_2]$ and $[Pt(cod)_2]$ (cod = *cis*,*cis*-1,5-cyclooctadiene) in toluene and subsequent annealing under a 50 bar H_2 pressure at 200 °C. Nanostructured thin films of the MnAl phase were electrochemically deposited from $AlCl_3$ and $MnCl_2$ in ionic liquids.[11] Some years ago, we were active in the field of precursor development for the metal organic chemical vapor deposition (MOCVD) of intermetallic thin films such as β-CoGa and ϵ-NiIn and we have noted there the possibility of MOCVD of CoAl thin films from organometallic single molecule precursors as well.[12] But none of these above routes holds immediate promise for a selective synthesis of *free-standing* soluble metal aluminide particles stabilized as a colloid, allowing further nanochemistry and processing. Furthermore, the decomposition pathways are usually complex and, as it appears at least to us, are not fully understood or documented in the literature.[13] In those cases, where the aluminum component is also used as the stoichiometric reducing reagent for the transition metal component, the M:Al ratio cannot be adjusted freely. The goal of our work is thus directed to overcome these limitations, and we intend to set up protocols to derive transition metal aluminide nanoparticles with full control over composition and particle size distribution under very clean conditions with as innocent and as few side products as possible, ideally using all-hydrocarbon precursors and hydrocarbon solvents under rigorously oxygen-free conditions. Our attention was thus drawn to *metastable* organometallic Al(I) compounds, namely, $(AlCp^*)_4$ (**1**, Cp* = C_5Me_5)[14] as the precursor for nano-Al.

Experimental Section

General Considerations and Analytical Methods. All manipulations and chemical reactions were conducted using Schlenk line and glovebox techniques (Ar, H_2O, O_2 < 1 ppm) and sealed Fischer−Porter vessels (100 mL). All powder X-ray diffractograms were recorded on a D8 Advance Bruker AXS diffractometer (Cu Kα radiation) in $\theta-2\theta$ geometry and a position sensitive detector (capillary technique under argon). Transmission electron microscopy (TEM) measurements were carried out on a Hitachi-H-8100 instrument (Accelerating voltage up to 200 kV, LaB_6-filament). High-resolution transmission electron microscopy (HRTEM) studies were performed at the Hahn-Meitner Institute in Berlin on a Philips CM30 instrument with an accelerating voltage up to 300 kV. All TEM samples were prepared on carbon coated gold grids. X-ray photoelectron spectroscopy (XPS) spectra were recorded on a Scienta Specs DEN-TECH UHV analysis system (the spectra were calibrated to C 1s at 284.5 eV; the sample was prepared in a glovebox and transferred to the ESCA via an inert gas transfer holder). Solid state ^{27}Al magic-angle spinning (MAS) NMR samples were recorded on a Bruker DSX 400 spectrometer in a 4 mm ZrO_2 rotor at 104.196 MHz (25 °C) with a rotation frequency of 5000 Hz, unless otherwise stated. All high-resolution NMR spectra in solution were recorded on a Bruker DPX 250 spectrometer in C_6D_6 and toluene-d_8 (T = 25 °C; ^{1}H, 250.1 MHz; ^{13}C, 62.9 MHz; ^{27}Al, 65.2 MHz; ^{31}P, 101.3 MHz). The chemical shifts (in ppm) are referenced to the residual proton signals of the deuterated solvent (C_6D_6 ^{1}H, 7.15 ppm; toluene-d_8 ^{1}H, 2.09 ppm) or the probe head (^{27}Al, 68 ppm, referenced to $[Al(H_2O)_6]^{3+}$ set at 0 ppm). UV−vis spectra were recorded on a Perkin-Elmer Lambda 9 UV/vis/near-infrared spectrometer. The samples were diluted in dry mesitylene and placed into quartz glass vials (1 cm path length) using a glovebox. IR measurements (KBr pellets) were carried out on a Perkin-Elmer 1720 X Fourier transform spectrometer. GC/MS measurements were performed on a Shimadzu GCMS-QP2010 using standard settings for hydrocarbon separation. The analysis for the metal content was undertaken using a Vario AAS 6 atomic absorption spectrometer. In situ NMR reactions were done using pressure stable NMR tubes with poly(tetrafluoroethylene) screw caps. The precursors $(AlCp^*)_4$ and $[CpCu(PMe_3)]$ were synthesized according to the literature.[14c,15] All used solvents were dried, degassed, and argon saturated by using a continuous solvent purification system (MBraun; H_2O, O_2 below 1 ppm). Poly(2,6-dimethyl-1,4-phenylene oxide) (PPO, powder) was purchased from Aldrich.

Nano-Al. A sample of **1** (1.000 g, 1.541 mmol) was suspended in mesitylene (10 mL) at 25 °C, pressurized with H_2 (3 bar), and heated to 150 °C (oil bath). After a few minutes, **1** was dissolved completely to give a yellow solution. After 15 min, a finely dispersed black suspension formed. The mixture was stirred for 1 h, whereupon the solution became colorless and the black solid precipitated. After cooling to 25 °C, the supernatant was decanted under argon, and the highly pyrophoric Al powder was washed with pentane (3 × 10 mL) and dried in vacuo. Yield: 160 mg (100%, according to Scheme 1). AAS: Al, 100%. ^{27}Al MAS NMR (Figure 5a): δ 1639 (Al^0). PXRD reflexes in 2θ (Figure 1): 38.53 (*hkl* 111; int. 100%), 44.81 (200, 39%), 65.25 (220, 22%), 78.36 (311, 20%), 82.58 (222, 6%). ^{1}H NMR (filtrate): δ 1.81 (s, 6 H, Cp*H, *meta*-CH_3), 1.74 (s, 6 H, Cp*H, *ortho*-CH_3), 0.99 (d, 3 H, Cp*H, *ipso*-CH_3).

(7) (a) Foley, T. J.; Johnson, C. E.; Higa, K. T. *Chem. Mater.* **2005**, *17*, 4086. (b) Jouet R. J.; Warren, A. D.; Rosenberg, D. M.; Bellitto, V. J.; Park, K.; Zachariah, M. R. *Chem. Mater.* **2005**, *17*, 2987.
(8) (a) Gladfelter, W. L.; Boyd, D. C.; Jensen, K. F. *Chem. Mater.* **1989**, *1*, 339. (b) Higa, K. T.; Johnson, C. E.; Hollins, R. A. U.S. Patent 5,885,321, 1999.
(9) Bönnemann, H.; Brijoux, W.; Hofstadt, H. W.; Ould-Ely, T.; Schmidt, W.; Wassmuth, B.; Weidenthaler, C. *Angew. Chem., Int. Ed.* **2002**, *41*, 599.
(10) Weidenthaler, C.; Brijoux, W.; Ould-Ely, T.; Spliethoff, B.; Bönnemann, H. *Appl. Organomet. Chem.* **2003**, *17*, 701.
(11) Endres, F.; Bukowski, M.; Hempelmann, R.; Natter, H. *Angew. Chem., Int. Ed.* **2003**, *42*, 3428.
(12) (a) Fischer, R. A.; Miehr, A. *Chem. Mater.* **1996**, *8*, 497. (b) Fischer, R. A.; Miehr, A.; Metzger, T. *Thin Solid Films* **1996**, *289*, 147. (c) Miehr, A.; Fischer, R. A.; Lehmann, O.; Stuke, M. *Adv. Mater. Opt. Electron.* **1996**, *6*, 27. (d) Fischer, R. A.; Kleine, M.; Lehmann, O.; Stuke, M. *Chem. Mater.* **1995**, *7*, 1863. (e) Fischer, R. A.; Miehr, A.; Schulte, M. M. *Adv. Mater.* **1995**, *7*, 58. (f) Fischer, R. A.; Behm, J.; Priermeier, T.; Scherer, W. *Angew. Chem., Int. Ed. Engl.* **1993**, *32*, 746.
(13) Bönnemann, H.; Brijoux, W.; Brinkmann, R.; Endruschat, U.; Hofstadt, W.; Angermund, K. *Rev. Roum. Chim.* **1999**, *44*, 1003.
(14) (a) Dohmeier, C.; Robl, C.; Tacke, M.; Schnöckel, H. *Angew. Chem., Int. Ed. Engl.* **1991**, *30*, 564. (b) Schulz, S.; Roesky, H. W.; Koch, H. J.; Sheldrick, G. M.; Stalke, D.; Kuhn, A. *Angew. Chem., Int. Ed. Engl.* **1993**, *32*, 1729. (c) Schormann, M.; Klimek, K. S.; Hatop, H.; Varkey, S. P.; Roesky, H. W.; Lehmann, C.; Röpken, C.; Herbst-Irmer, R.; Noltemeyer, M. *J. Solid State Chem.* **2001**, *126*, 225.
(15) Werner, H.; Otto, H.; Ngo-Khac, T.; Burschka, C. *J. Organomet. Chem.* **1984**, *262*, 123.

Scheme 1. Hydrogenolysis of $(AlCp^*)_4$ (1) and Reaction with ^{i}Bu$_2$AlH To Yield Nano-Al Particles

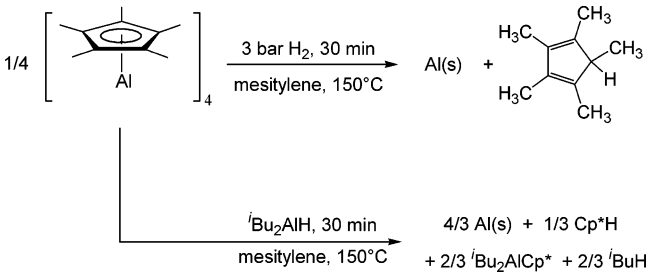

$CuAl_2$. Samples of **1** (0.159 g, 0.245 mmol) and **2** (0.100 g, 0.488 mmol) were combined in mesitylene (10 mL), treated with 3 bar H_2, and set into a 150 °C hot oil bath. After a few minutes, the yellow solution became darker, and after 15 min, a gray precipitate formed. After 3 h of stirring at 150 °C the precipitated gray $CuAl_2$ powder was isolated as described above. Yield: 55 mg (96%, according to Scheme 2). AAS: Al, 65.3%; Cu, 32.5%. EDX analysis: Al, 69%; Cu, 31%. ^{27}Al MAS NMR (Figure 5b): δ 1486. PXRD data are listed in Table 1. ^{1}H NMR (filtrate): δ 6.50 (s, 2 H, CpH, *meta*-CH_2), 6.36 (s, 2 H, CpH, *ortho*-CH_2), 1.81 (s, 6 H, Cp*H, *meta*-CH_3), 1.74 (s, 6 H, Cp*H, *ortho*-CH_3), 0.99 (d, 3 H, Cp*H, *ipso*-CH_3), 0.81 (d, 9 H, P(CH_3)$_3$).

Cu Colloids.[23] In a Fischer−Porter bottle, 0.100 g of **2** (0.488 mmol) and 0.310 g of PPO were dissolved in mesitylene (20 mL). The slight yellow solution was degassed and set to 3 bar H_2. The bottle was then placed into an oil bath set to 150 °C. After 5 min the solution became light red; soon after, the characteristic wine red solution of Cu colloids was observed. The solution was stirred for 2 h at 150 °C. After cooling to room temperature, the solution was transferred into a Schlenk tube. The UV−vis spectrum is presented in Figure 6e.

$Cu_{1-x}Al_x$ Colloids. Samples of **1** and **2** with the desired molar ratio ($0.10 \le x \le 0.50$), for example, $x = 0.33$, which refers to 0.025 mmol of **1** and 0.244 mmol of **2**, were combined in mesitylene (40 mL). A sample of PPO (0.188 g) was added, and the mixture was treated with stirring under 3 bar H_2 at 150 °C for 16 h. From the deeply red-colored colloidal solutions, the PPO stabilized $Cu_{1-x}Al_x$ particles were quantitatively precipitated by addition of *n*-hexane (100 mL), washed with *n*-hexane, quantitatively redispersed in toluene or mesitylene again, and characterized by TEM and energy-dispersive X-ray (EDX) analysis. EDX analysis. Calcd for $Cu_{1-x}Al_x$: $x = 0.50$. Found: Al, 0.54; Cu, 0.46. Calcd: $x = 0.33$. Found: Al, 0.30; Cu, 0.70. Calcd: $x = 0.17$. Found: Al, 0.19; Cu, 0.81. Calcd: $x = 0.10$. Found: Al, 0.08, Cu, 0.92. ^{27}Al MAS NMR (Figure 5c) for sample $Cu_{0.50}Al_{0.50}$, δ 1446. The ^{27}Al NMR shifts for the more copper-rich samples could not be detected so far, possibly because of extreme relaxation times. The powder X-ray diffraction (PXRD) data of all samples $Cu_{1-x}Al_x$ are given in Figure 5, and for the related UV−vis spectra, see Figure 6.

Reaction of AlCp* with ^{i}Bu$_2$AlH. $(AlCp^*)_4$ (0.500 g, 0.771 mmol) was dissolved in mesitylene (30 mL) at 150 °C and treated with a 1 M solution of ^{i}Bu$_2$AlH in tetrahydrofuran (3.1 mL, 3.100 mmol). Immediately, a black solid precipitated. The mixture was stirred for 16 h at 150 °C. After cooling to room temperature, the solution was filtered, and the black solid was washed with pentane (2×20 mL), dried, and identified as Al by PXRD. Yield: 0.055 g (2.055 mmol, referring to 66% yield supporting the stoichiometry of Scheme 1). For a quantitative detection of [Cp*Al^{i}Bu$_2$], Cp*H, and isobutane, a NMR reaction was performed: $(AlCp^*)_4$ (0.050 g, 0.077 mmol) and ^{i}Bu$_2$AlH (0.308 mL, 1 M solution in toluene) were suspended in toluene-d_8 (1 mL) and heated at 120 °C for 2 h. After a few minutes, Al(0) precipitated. In the recorded ^{1}H NMR spectrum, the signals of [Cp*Al^{i}Bu$_2$] were visible at 1.86 ppm (s, 15 H, Cp*), 0.98 ppm (m, 12 H, $-CH_2-CH-(CH_3)_2$), and −0.13 ppm (m, 4 H, $-CH_2-CH-(CH_3)_2$). The signals of the rest of the Cp*H appeared at 1.78 ppm (d, 3 H) and 1.71 ppm (d, 3 H) and matched the expected ratio [Cp*Al^{i}Bu$_2$]/Cp*H of 1:0.5. The proton signals at the aliphatic carbon of the Cp* ring could not be detected because of overlapping signals of [Cp*Al^{i}Bu$_2$]. The methyl proton signal of isobutane appeared at 1.08 ppm (m, 9 H, CH(CH_3)$_3$) and also matched the expected ratio [Cp*Al^{i}Bu$_2$]/isobutane of 1:1. The proton at the tertiary carbon, which should appear at around 1.8 ppm, was not visible as a result of other signals lying above. The ^{27}Al NMR spectrum exhibited a signal of [Cp*Al^{i}Bu$_2$] at −86.9 ppm.

Results and Discussion

Al Nanoparticles from $(AlCp^*)_4$ by Hydrogenolysis. Treatment of **1** dissolved in mesitylene ($c = 0.15$ mol/L) with 3 bar H_2 at 150 °C yields 160 mg of a pyrophoric black precipitate already after 15 min, which was identified as analytically pure aluminum (elemental analysis; PXRD, Figure 1). The reaction is clean and quantitative according to ^{1}H NMR and GC/MS studies of the supernatant (Scheme 1). The ^{1}H NMR spectrum of the filtrate of the reaction mixture exhibits the expected three signals of the methyl protons of Cp*H (two singlets at 1.81 and 1.74 ppm, as well as a doublet at 0.99 ppm in a ratio of 6:6:3). The signal of the proton at the aliphatic ring carbon was not detected because of the low concentration of the sample in the original filtrate. Correspondingly, the ^{27}Al NMR spectrum of the filtrate did not show any signals. Hence, a formation of any Al(III) species during the hydrogenolysis of AlCp* as well as the presence of unchanged **1** or other Al(I) species can be excluded.

Matrix isolation Fourier transform infrared studies and quantum chemical calculations reported by Himmel and Vollet revealed that the photoinduced reaction of monomeric AlCp* with H_2 in an argon matrix at 12 K yields the dimer [Cp*Al(μ-H)]$_2$.[16] That species may also play a role in the hydrogenolysis described above, because the tetrahedral cluster of **1** undergoes a dissociation/association equilibrium with monomeric AlCp* at elevated temperatures in solution.[17] To shine some light into the hydrogenolysis mechanism of **1** and because of the so far synthetic inaccessibility of [Cp*AlH$_2$] as a possible intermediate, we treated **1** with ^{i}Bu$_2$-

(16) Himmel, H.-J.; Vollet, J. *Organometallics* **2002**, *21*, 5972.
(17) Dohmeier, C.; Loos, D.; Schnöckel, H. *Angew. Chem., Int. Ed. Engl.* **1996**, *35*, 129.
(18) Timoshkin, A. Y.; Frenking, G. *J. Am. Chem. Soc.* **2002**, *124*, 7240.
(19) As a result of the magnetization of metallic powder in the field of the MAS NMR instrument, the minimal spin frequency of 5000 Hz, required for a measurement, could not be reached. Therefore, the samples were diluted in PPO to separate the single particle grains and avoid the magnetization effect.
(20) (a) Müller, D.; Gessner, W.; Behrens, H.-J.; Scheler, G. *Chem. Phys. Lett.* **1981**, *79*, 59. (b) Kunath-Fandrei, G.; Bastow, T. J.; Hall, J. S.; Jäger, C.; Smith, M. E. *J. Phys. Chem.* **1995**, *99*, 15138.
(21) (a) Bastow, T. J.; Smith, M. E. *J. Phys.: Condens. Matter* **1995**, *7*, 4929. (b) Reference measurements were performed at the Ruhr-University Bochum with Al powder (Fluka) and Al_2O_3 (neutral, for column chromatography, Merck). The Al(0) signal appeared at 1640 ppm, and the two Al_2O_3 signals were found at 68 and 8 ppm.
(22) Cokoja, M.; Fischer, R. A. Unpublished results.
(23) Cokoja, M.; Schröter, M. K.; Parala, H.; van den Berg, M. W. E.; Klementiev, K. V.; Grünert, W.; Birkner, A.; Fischer, R. A. Manuscript in preparation.

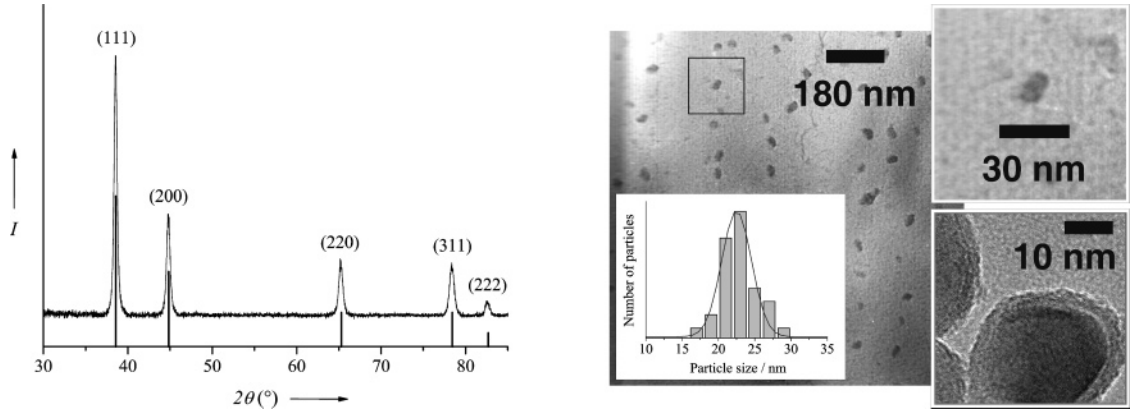

Figure 1. PXRD pattern (left, lines: JCPDS reference data no. 4-0787) and TEM images (right) of the nano-Al powder obtained according to Scheme 1.

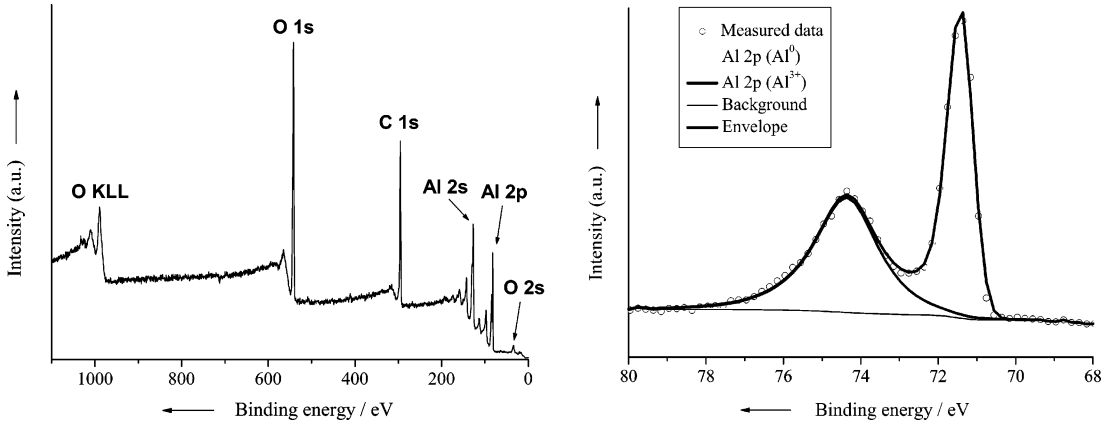

Figure 2. XPS spectra of Al nanoparticles (left, survey; right, Al region).

AlH at 150 °C in mesitylene. Immediate precipitation of aluminum occurred, and the observed byproducts Cp*H and Al^iBu_3 are likely to stem from the decomposition of the intermediate adduct $[^iBu_2(H)Al^{III}-Al^ICp^*]$. According to theoretical studies by Timoshkin and Frenking,[18] this latter compound is very likely to be rather unstable under our conditions and is thought to rapidly decompose according to Scheme 1. At the very least, the stoichiometry of the hydrogenolysis of **1** (Scheme 1) being based on a mass-balance and identification (NMR, GC/MS) of all products substantiates our suggestions.

It is of course important to explicitly state here that neither AlR_3 (R = Me, Et), nor $^iBu_2AlH$ as the most obvious alternative Al precursors decomposes to yield aluminum particles under rather mild conditions of 3 bar H_2 at 150 °C in mesitylene over a period of several hours of treatment. The treatment of $[Me_3N-AlH_3]$ with 3 bar H_2 does lead to elemental aluminum; however, the decomposition occurs significantly slower (ca. 1 h) than in the case of **1**, and the particles are around 50 nm in length (PXRD) with a very broad size distribution. Also we wish to point out that we deliberately avoided using any catalyst such as $[Ti(O^iPr)_4]$ as reported by Higa et al.[7a,8] for the sake of most clean conditions and the reducing of byproducts of any kind. With these constraints in mind, the hydrogenolysis of **1** with Cp*H as the only and chemically rather inert byproduct was selected for nanometallurgy of aluminides, rather than the more complex reduction of **1** with $^iBu_2AlH$ or any alternative aluminum reagent with or without a catalyst.

The TEM images of the Al powder obtained by hydrogenolysis of **1** show surprisingly uniform, in the (111) direction elongated particles of 23 ± 2 nm matching the estimation from the PXRD reflex broadening based on the Scherrer equation (Figure 1). XPS proves the presence of Al(0) ($2p_{3/2}$ peak at 71.4 eV) and Al(III) ($2p_{1/2}$ peak at 74.4 eV), pointing to Al_2O_3, and a close-up of a selected particle points to a 3 nm thick amorphous coating around the nanocrystalline Al core (Figures 1 and 2).

Bare nano-Al is, of course, a getter for oxygen. The ^{27}Al MAS NMR spectrum (Figure 5a) of a sample being freshly synthesized (glovebox, Ar, solvents with O_2, H_2O < 1 ppm), diluted with PPO[19] and immediately transferred into a ZrO_2 rotor and sealed, exhibited only traces of the Al_2O_3 signals at 1.0 ppm (AlO_6) and 57.0 ppm (AlO_4)[20] besides the easily observed Knight Shift resonance at 1639 ppm, which perfectly matches the Al metal shifts reported in the literature as well as our own reference measurements.[21] No other ^{27}Al signals were detected, and similarly, hydrocarbon impurities were absent according to ^1H MAS NMR and IR data (KBr pellet).

We conclude that **1** has significant potential as a very clean and controllable source for bare nano-Al particles in non-aqueous, aprotic solution. It should be noted here that the heavier congeners of $(AlCp^*)_4$, $(GaCp^*)_6$, and $(InCp^*)_6$ also decompose when treated with 3 bar H_2 pressure under the same conditions as described, to yield elemental gallium and indium, respectively, and Cp*H as a side product.[22] While $(InCp^*)_6$ decomposes as fast as $(AlCp^*)_4$ (within minutes),

Scheme 2. Co-Hydrogenolysis of $(AlCp^*)_4$ (1) and $[CpCu(PMe_3)]$ (2) and Wet-Chemical Synthesis of $CuAl_2$ and $Cu_{1-x}Al_x$ Colloids, Stabilized by PPO

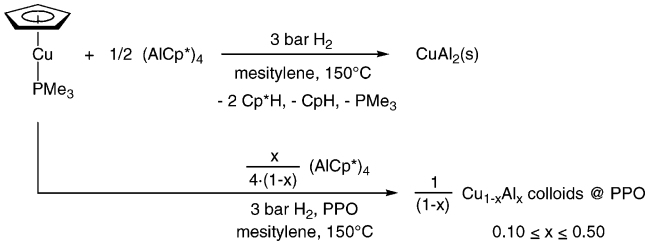

Table 1. Comparison of PXRD Reflexes (2θ, deg) of Synthesized $CuAl_2$ and Reference Data (JCPDS No. 25-0012)

hkl (int. in %)	our $CuAl_2$ sample	$CuAl_2$ reference	*hkl* (int. in %)	our $CuAl_2$ sample	$CuAl_2$ reference
110 (100)	20.681	20.620	004 (8)	78.406	78.382
200 (35)	29.474	29.386	510 (11)	81.162	80.678
211 (70)	38.010	37.867	422 (11)		81.007
220 (35)	42.200	42.071	431 (9)	82.440	81.842
112 (90)	42.683	42.591	114 (9)		82.181
310 (70)	47.442	47.332	204 (1)	86.119	85.950
202 (60)	47.910	47.808	521 (5)	89.429	89.103
222 (13)	57.257	57.129	413 (3)	90.096	89.829
400 (2)	61.646	61.032	440 (3)	92.056	91.872
312 (6)		61.435	512 (5)	93.283	92.205
411 (6)	66.404	66.335	324 (3)	93.505	93.220
213 (9)	67.214	67.034	530 (2)	95.778	95.577
420 (11)	69.330	69.173	314 (17)	97.184	97.063
402 (21)	73.620	73.462	600 (5)	99.542	99.267
332 (20)	77.483	77.251			

$(GaCp^*)_6$, surprisingly, decomposes only very slowly after 2 days of treatment with 3 bar H_2 at 150 °C.

Nanocrystalline $CuAl_2$ Powder by Co-Hydrogenolysis of 1 with 2. Aiming at the development of a generally applicable soft chemical synthesis of transition metal aluminide colloids in nonaqueous solution, we selected the Cu/Al system as our test case, as explained in the introduction. A suitable Cu source is $[CpCu(PMe_3)]$ (**2**, Cp = η^5-C_5H_5).[15] Its hydrogenolysis yields analytically pure Cu(0), on which chemistry we will report in more detail elsewhere.[23] The ligands Cp and PMe_3 are easily cleaved from the copper center of **2**, releasing Cu atoms that neither undergo side reactions nor adsorb noticeably to the surface of the growing particles (NMR). Furthermore, CpH and PMe_3 are not prone to be transferred to the Al side in contrast to acetylacetonate or halide as the typical ligands, for example, used in the Bönnemann synthesis of copper colloids, which typically uses $[M(acac)_2]$ as the metal source and AlR_3 as both the reducing agent *and* the surfactant.[13,24] The co-hydrogenolysis of **1** and **2** with a Cu/Al molar ratio of 1:2 yields a gray, surprisingly air stable, nonpyrophoric precipitate and a clear colorless supernatant (Scheme 2).

Elemental analysis and PXRD of the powder as-synthesized proved the formation of θ-$CuAl_2$ (Khatyrkite, tetragonal body-centered *I*4/*mcm*). The PXRD pattern perfectly matched reference data (Figure 3). The Cu/Al ratio of 1:2 was confirmed by EDX analysis of a TEM sample of our $CuAl_2$ material. The average particle size was calculated to be 35 ± 5 nm via the Scherrer equation. A hint on the rather small grain size of the obtained powder was the diffraction pattern, which exhibited relatively broad reflexes (fwhm of the 110 reflex: $2\theta = 0.289°$), compared to a highly crystalline, annealed reference sample (fwhm of 110 reflex: $2\theta = 0.143°$).[25] The peak broadening was demonstrated in six reflexes, which were expected to appear as three pairs at 2θ = 61.032, 61.435, 80.678, 81.007, 81.842, and 82.181, but could not be fully resolved because of overlapping and emerged as three broadened reflexes at 61.646, 81.162, and 82.440 in 2θ, respectively. The reaction was performed at 150 °C, and further annealing of the sample was not intended giving rise to further particle growth, peak sharpening, and crystallization. So we can certainly not exclude the co-formation of any other amorphous Cu/Al phases by PXRD. The TEM image revealed agglomerated particles with a broad size distribution of around 100 nm, which is not surprising, as the precursors were decomposed without any surfactant present, which would prevent agglomeration.

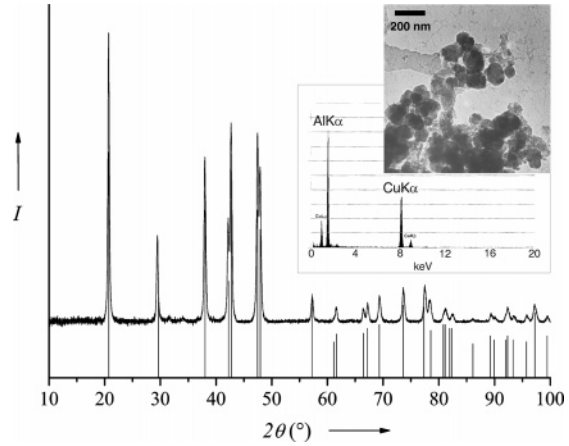

Figure 3. PXRD diffractogram of $CuAl_2$ synthesized according to Scheme 2 (reference data JCPDS no. 25-0012) and TEM/EDX images (inset, bar = 200 nm).

The Al−Cu phase diagram[26] is as complex as the Cu−Zn brass system, containing the typical regions of the α, β, and γ phases at the Cu-rich side and exhibiting several intermetallic compounds with distinct solid state structures and crystallographic properties, namely, Cu_3Al, Cu_9Al_4, Cu_4Al_3, CuAl, and θ-$CuAl_2$, at specific conditions of existence. Thus, looking at the Cu-rich side of the phase diagram between the α phases that have Cu structure and θ-$CuAl_2$, it is obvious that it is difficult to prepare a phase pure copper aluminide compound $Cu_{1-x}Al_x$, with $0.25 \leq x \leq 0.50$. In particular, the formation of Cu_9Al_4 and $CuAl_2$ is often observed in typical ball milling[27] and interfacial reactions.[28] Depending on the conditions, other intermetallic Cu/Al compounds, that

(24) (a) Bönnemann, H.; Botha, S. S.; Bladergroen, B.; Linkov, V. M. *Appl. Organomet. Chem.* **2005**, *19*, 768. (b) Vukojević, S.; Trapp, O.; Grunwaldt, J.-D.; Kiener, C.; Schüth, F. *Angew. Chem., Int. Ed.* **2005**, *44*, 7978.

(25) The $CuAl_2$ sample (^{27}Al Knight Shift: 1480 ppm), donated by Prof. Dr. Yuri Grin, was measured at the Ruhr-University Bochum under the same conditions as all other solid state NMR and PXRD samples, as described in Experimental Section.

(26) Hansen, M. *Constitution of binary alloys*, 2nd ed.; McGraw-Hill: New York, 1969.

(27) (a) Ying, D. Y.; Zhang, D. L. *J. Alloys Compd.* **2000**, *311*, 275. (b) Xi, S. Q.; Qu, X. Y.; Ma, M. L.; Zhou, J. G.; Zheng, X. L.; Wang, X. T. *J. Alloys Compd.* **1998**, *268*, 211.

(28) Jiang, H. G.; Dai, J. Y.; Tong, H. Y.; Ding, B. Z.; Song, Q. H.; Hu, Z. Q. *J. Appl. Phys.* **1993**, *74*, 6165. (b) Umakoshi, Y.; Fujitani, W. *J. Jpn. Inst. Met.* **1994**, *58*, 1095.

is, Cu_3Al, Cu_4Al_2, and CuAl, mentioned above are detected, too.[29] Of particular interest in our context are the well-studied thin film reactions of Cu/Al multilayers which had been investigated by Jiang et al. using differential scanning calorimetry and TEM. Sequential intermetallic compound formation was found in the temperature range from 27 to 347 °C, somewhat matching our conditions in solution. The activation energies for the formation of $CuAl_2$ and Cu_9Al_4 were determined to be 0.78 ± 0.11 and 0.83 ± 0.2 eV, respectively. The $CuAl_2$ phase was formed *prior* to the Cu_9Al_4 phase even in the presence of excess copper.[28a] For example, the co-decomposition of **1** and **2** in an Al/Cu ratio of 4:9 under 3 bar H_2 at 150 °C and keeping the reaction mixture under those conditions for 1 week did not yield the Cu_9Al_4 phase similarly to $CuAl_2$. In the PXRD of the obtained powder, only broad Cu reflexes were detected. By annealing the isolated powder to 500 °C in vacuo for 5 days, the characteristic reflections of Cu_9Al_4 emerged gradually. This comparison may explain why it is possible to obtain apparently phase-pure θ-$CuAl_2$ particles rather than a more complex mixture together with Cu_9Al_4 and other possible compounds by our organometallic route. At very low temperatures of 150 °C the alloying process is certainly kinetically controlled.

The ^{27}Al Knight Shift resonance at 1486 ppm of the $CuAl_2$ material is clearly shifted to high field from pure aluminum at 1639 ppm (Figure 5b) and exactly corresponds to the Al shift observed by the groups of Bastow[30] and Torgeson,[31] as well as to our own $CuAl_2$ reference measurements.[25] The Knight Shift is a sensitive probe for the local electronic density of states, reflecting different crystallographic aluminum sites, and, thus, the qualitative change of the isotropic value of the Knight Shift resonance unambiguously indicates alloying of Al with Cu in our case. Interestingly, traces of oxygen, being certainly present (see the TEM of Al particles in Figure 1), are no obstacle for alloying. Again, hydrocarbon impurities are absent (^{1}H MAS NMR and IR). The byproducts according Scheme 2 were found by GC/MS, ^{1}H NMR, and ^{31}P NMR. In the ^{1}H NMR spectrum of the filtrate of the reaction mixture, the three typical resonances of Cp*H methyl protons are observed again, similar to the pure Al case above (1.81 (s), 1.74 (s), and 0.99 ppm (d) in a ratio of 6:6:3). The olefinic protons of cyclopentadiene (CpH) are observed at 6.50 (s) and 6.36 ppm (s). In analogy to Cp*H, the aliphatic proton of CpH is not visible. Besides, the resonances at 0.81 ppm (d, J_{P-H} (Hz) = 2.585) are assigned to the free PMe_3 ligand, and in the ^{31}P NMR spectrum, the signal of the P atom expectedly appears at −62.4 ppm. A quantitative NMR experiment (sealed tube) was performed under conditions similar to those as described above. The signal intensities matched the stoichiometry presented in Scheme 2.

Synthesis and Characterization of $Cu_{1-x}Al_x$ Colloids. The results described above proved the suitability of **1** as an Al source for alloying with Cu. We then turned our interest toward the synthesis of α-CuAl, respectively $Cu_{1-x}Al_x$ alloy colloids ($0.10 \leq x \leq 0.50$). The choice of an appropriate surfactant, weakly adsorbing at the particle surface and controlling Ostwald ripening, is crucial for this purpose. Whereas pure Cu particles can be very easily stabilized with a variety of surfactants, including hexadecylamine (HDA),[32] our particular aluminum precursor, $(AlCp^*)_4$ (**1**) (similarly to other obvious aluminum sources mentioned in the introduction) appeared to be much too reactive toward all the usual choices of capping ligands; for example, **1** reacts with HDA under H_2 pressure to yield an Al(III) amide. Similarly, other common surfactants are either too reactive against **1** and/or nano-Al, for example, oleic acid, trioctylphosphineoxide and poly(vinylpyrrolidone), or failed to keep the particles in solution (e.g., long chain tertiary amines and phosphines). Alkyl chain polyethers of the type $RO-(CH_2CH_2O)_nR$ introduce the problem of traces of water, which are very difficult to rigorously reduce below the level of 1 ppm. Thus, we selected a related polymeric stabilizer, PPO, which is also a widely used surfactant in colloid synthesis,[33] that proved to behave inertly toward **1** (NMR). However, even using PPO, we so far were unable to derive a $CuAl_2$ ($Cu_{0.33}Al_{0.67}$) nanomaterial being composed of nonaggregated, individual $CuAl_2$ particles dispersed in a colloidal solution. The same is true for all our efforts to obtain well-defined pure nano-Al colloids in mesitylene, stabilized by PPO. But by reducing the Al content to $x \leq 0.50$, the co-hydrogenolysis of **1** and **2** in molar ratios from 1:1 to 1:9 in the presence of PPO resulted in nicely deep red-colored $Cu_{1-x}Al_x$ colloids ($0.10 \leq x \leq 0.50$), which could be precipitated with pentane and, thereafter, fully redispersed in toluene or mesitylene by ultrasound. All these novel $Cu_{1-x}Al_x$ colloids exhibited a rather broad particle size distribution of around 16 ± 5 nm (for $x = 0.50$, 17 ± 5 nm; $x = 0.33$, 16 ± 3 nm; $x = 0.17$, 18 ± 4 nm; $x = 0.10$, 18 ± 5 nm; see Figure 6). Apparently, the solubility of alloyed Cu/Al−PPO particles in mesitylene increases with a rising Cu content on moving away from intermetallic compounds such as $CuAl_2$ and toward the solid solution α-CuAl phase. We observed a similar behavior for related nanobrass α/β-CuZn particles stabilized by PPO, with the best solubility observed for α-CuZn particles rather than β-CuZn and so forth.[23] Noteworthy is that the solubility of PPO and the $Cu_{1-x}Al_x$ particles improved using anisole as the solvent rather than mesitylene. Consequently, it is more difficult to precipitate the particles from an anisole solution than from mesitylene. EDX spectroscopy of the precipitated, washed, and redispersed $Cu_{1-x}Al_x$ particles revealed the expected compositions of the particles close to the expected ratio of the metals within the accuracy of the not deliberately calibrated method (10% relative error).

(29) (a) Abbasi, M.; Taheri, A. K.; Salehi, M. T. *J. Alloys Compd.* **2001**, *319*, 233. (b) Draissia, M.; Boudemagh, H.; Debili, M. Y. *Phys. Scr.* **2004**, *69*, 348.
(30) Bastow, T. J.; Celotto, S. *Acta Mater.* **2003**, *51*, 4621.
(31) Torgesson, D. R.; Barnes, R. G. *J. Chem. Phys.* **1975**, *62*, 3968.
(32) (a) Hambrock, J.; Becker, R.; Birkner, A.; Weiss, J.; Fischer, R. A. *Chem. Commun.* **2002**, 68. (b) Schröter, M. K.; Khodeir, L.; Hambrock, J.; Löffler, E.; Muhler, M.; Fischer, R. A. *Langmuir* **2004**, *20*, 9453.
(33) (a) Dassenoy, F.; Casanove, M.-J.; Lecante, P.; Verelst, M.; Snoeck, E.; Mosset, A.; Ould Ely, T.; Amiens, C.; Chaudret, B. *J. Chem. Phys.* **2000**, *112*, 8137. (b) De Caro, D.; Ould Ely, T.; Mari, A.; Chaudret, B.; Snoeck, E.; Respaud, M.; Broto, J.-M.; Fert, A. *Chem. Mater.* **1996**, *8*, 1987.

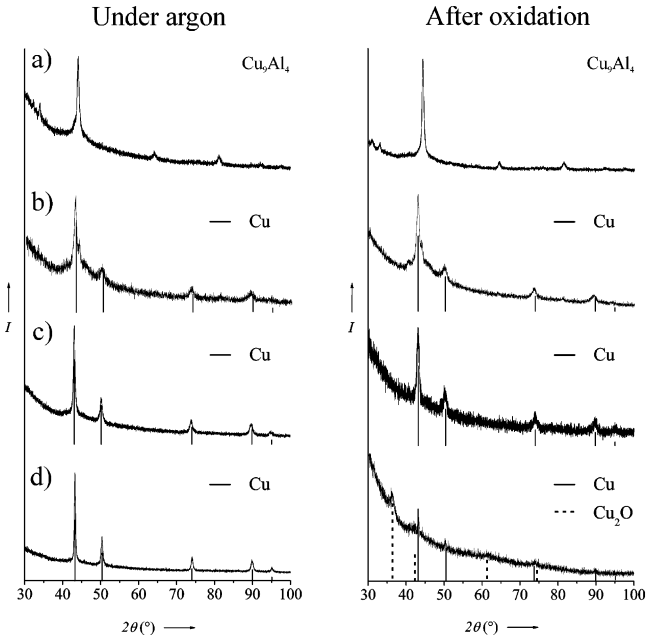

Figure 4. PXRD diagrams of PPO stabilized colloids of (a) $Cu_{0.50}Al_{0.50}$, (b) $Cu_{0.67}Al_{0.33}$, (c) $Cu_{0.83}Al_{0.17}$, and (d) $Cu_{0.90}Al_{0.10}$, measured under argon and on air (oxidation of the colloids before precipitation). Reference JCPDS data: Cu, 4-0836; Cu_9Al_4, 24-0003; Cu_2O, 5-0667.

Table 2. Deviation of the PXRD Reflexes of α-Cu/Al Phases from the Cu Structure (in 2θ, deg), in Dependence of the Al Content

reflex	111	200	220	311	222
Cu	43.298	50.434	74.132	89.934	95.143
$Cu_{0.9}Al_{0.1}$	−0.074	−0.094	−0.057	−0.093	−0.046
$Cu_{0.83}Al_{0.17}$	−0.160	−0.208	−0.242	−0.250	−0.209
$Cu_{0.67}Al_{0.33}$	−0.302	−0.365	−0.582	−0.662	−0.658

Unlike the $Cu_{0.33}Al_{0.67}$ ($CuAl_2$) case above, the PXRD pattern of the PPO stabilized $Cu_{0.50}Al_{0.50}$ (CuAl) particles could not be assigned to the expected CuAl phase (Cupalite, monoclinic *C*2/*m*, JCPDS no. 26-0016) but rather to Cu_9Al_4 (Figure 4a, cubic $P\bar{4}3m$, JCPDS no. 24-0003). Surprisingly, only the high-temperature phase Cu_9Al_4 was visible in the PXRD of colloidal $Cu_{0.50}Al_{0.50}$ under these reaction conditions. A powder sample prepared by combining **1** and **2** in the equimolar Cu/Al ratio without PPO exhibited reflections indexed for CuAl, Cu_2Al, Cu_3Al, Cu_4Al_3, and Cu_3Al_4 besides Cu_9Al_4. Hence, in the PXRD of the colloidal $Cu_{0.50}Al_{0.50}$ sample, the other possible, typically Al-rich phases were presumably amorphous; at least we cannot rule out this. Thus, the "$Cu_{0.50}Al_{0.50}$" sample should be regarded as a possible mixture of several Cu/Al α and β phases. Instead, the PXRD diagrams of precipitated $Cu_{1-x}Al_x$ colloids ($0.10 \leq x \leq 0.33$, Figure 4b−d) exhibited reflexes that could clearly be assigned to the typical fcc Cu pattern with slightly shifted Cu reflexes, caused by the random incorporation of Al atoms into the copper lattice forming a solid solution and thus corresponding to the α-phase region. The shift of the reflexes is expectedly proportional to the Al content in the samples (Table 2). Noteworthy is that in the PXRD diagram of the α-$Cu_{0.67}Al_{0.33}$ sample, the (330) reflex of Cu_9Al_4 at $2\theta = 44.075°$ (int. 100%) was observed besides the Cu reflexes (Figure 4b), indicating the coexistence of α and β phases. Other reflexes of Cu_9Al_4 were not visible because of the low intensity of this phase in the sample. Upon oxidation, the Cu_9Al_4 reflex remained unchanged, most likely due to the formation of a passivating alumina layer, as it was the case with $CuAl_2$; see discussion to follow.

In the ^{27}Al MAS NMR measurement of $Cu_{0.50}Al_{0.50}$, we observed a Knight Shift resonance of 1446 ppm, which is moved high-field from $Cu_{0.33}Al_{0.67}$, and matching of the trend from Al over $CuAl_2$ to CuAl with rising Cu content (Figure 5c). Correspondingly, upon oxidation, the ^{27}Al Knight Shift resonance of the metallic Al component became too weak to be detected, whereas the Al oxide signals rose (Figure 5d) and remained unchanged even after several hours of reduction at elevated temperatures (150 °C with H_2 or CO at 3 bar). Yet in the $Cu_{1-x}Al_x$ samples with an Al content of $x < 0.50$, we were unable to detect the Al metal signal, most probably because of the low Al concentration, caused by the dilution of the NMR samples by PPO together with increased relaxation time complications.

The alloying was also reflected by the transformation of the characteristic 573 nm surface plasmon resonance (SPR) of the pure Cu reference colloid[23] into a very broad absorption structure centered at 520 nm for the $Cu_{0.50}Al_{0.50}$ sample (Figure 6a). With rising Cu content, the absorption became more distinctly visible, and for $Cu_{0.67}Al_{0.33}$, a well-developed absorption peak at 519 nm was observed (Figure 6b). The typical SPR of nano-Cu appeared again at 573 nm with reduction of the Al mole fraction down to 10% in $Cu_{1-x}Al_x$ ($0.10 \leq x \leq 0.33$, Figure 6c,d). For our previously reported nanobrass colloids, for example, α-CuZn (5 atom % and 30 atom % Zn) and γ-CuZn (65 atom % Zn), we have observed a similar behavior with the SPR peak for the α-CuZn particles being close to the position of the pure Cu nanoparticles, while the γ-CuZn particles, having a rather high Zn content, have not revealed a significant SPR absorption feature.[4] The optical absorption spectra of metallic nanoparticles can be described according Mie's theory,[34] which gives the total extinction coefficient κ according to eq 1

$$\kappa = \frac{18\pi N V \epsilon^{3/2}}{\lambda} \frac{\epsilon_2}{[\epsilon_1 + 2\epsilon_m]^2 + \epsilon_2^2} \qquad (1)$$

where λ is the wavelength of the absorbing radiation and ϵ_m is the dielectric constant of the surrounding medium (assumed to be frequency independent). The values ϵ_1 and ϵ_2 are the real and imaginary parts of the complex dielectric function $\epsilon(\omega)$ of the material. As a result of the lack of suitable reference data, at least to our knowledge, for the bulk dielectric function of the various Cu/Al phases being involved in our study, we could not directly model the observed SPR spectra, so far. However, for example, a related simulation is possible for β-CuZn (with 50 atom % Zn) based on the data of the bulk dielectric function of β-brass[35] and reveals a matching of the observed absorption around 525−535 nm with the calculated maximum at 520 nm for β-CuZn.[36] In accordance, UV−vis spectra of our β-brass colloids, made by co-decomposition of **2** and [$ZnCp^*_2$] in PPO/mesitylene under hydrogen pressure, exhibited an

(34) Mie, G. *Ann. Phys.* **1908**, *25*, 377.
(35) Sasovskaya, I. I.; Korabel, V. P. *Phys. Status Solidi B* **1986**, *184*, 621.
(36) Suzuki, N.; Ito, S. *J. Phys. Chem. B* **2006**, *110*, 2084.

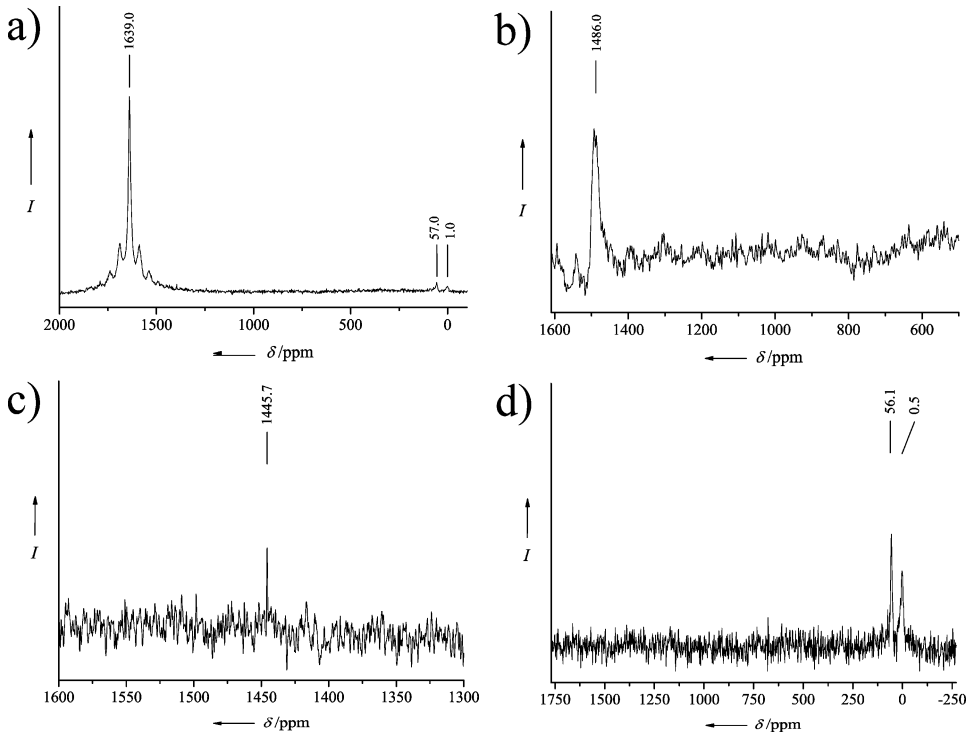

Figure 5. ^{27}Al MAS NMR of (a) Al nanoparticles, (b) $CuAl_2$ powder obtained by hydrogenolysis of **1** and **2**, (c) $Cu_{0.50}Al_{0.50}$@PPO colloids, and (d) oxidized $Cu_{0.50}Al_{0.50}$@PPO colloids (10 000 Hz).

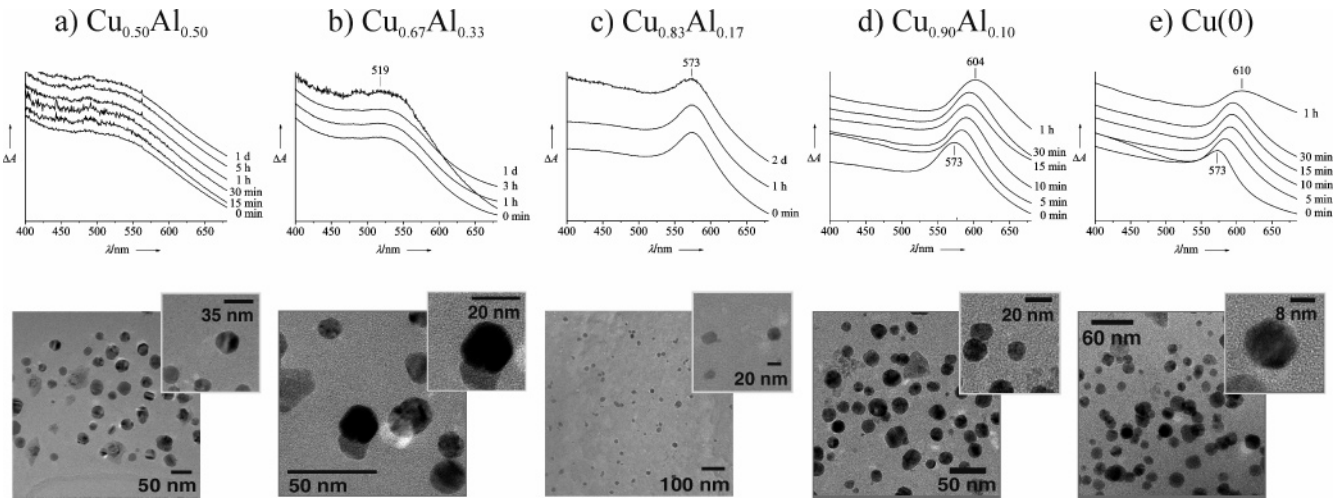

Figure 6. Time dependent oxidation of PPO stabilized colloids of (a) $Cu_{0.50}Al_{0.50}$, (b) $Cu_{0.67}Al_{0.33}$, (c) $Cu_{0.83}Al_{0.17}$, (d) $Cu_{0.90}Al_{0.10}$, and (e) pure Cu colloids@PPO, monitored by UV−vis spectroscopy (top). Bottom: TEM images of samples a−e.

absorption at 535 nm.[23] Assuming that the bulk dielectric functions of α/*β*-CuAl and α/*β*-CuZn are not fundamentally different, we may conclude that the observed shift of the SPR as a function of the composition clearly indicates alloy $Cu_{1-x}Al_x$ particles. In addition, it should be noted here that the particle size distribution has some influence also and the SPR shifts to longer wavelengths with increasing particle size, giving rise to substantial peak broadening, which may be especially important at higher Al contents.

Oxidation of $Cu_{1-x}Al_x$ Colloids and Formation of Core Shell Particles. Interestingly, even after a few days of exposure to ambient conditions (moist air), the UV−vis absorption of these $Cu_{1-x}Al_x$ colloids ($0.17 \leq x \leq 0.50$) did not change at all (Figure 6), quite similar to our related observations in the case of $Cu_{1-x}Zn_x$ alloy particles.[23] This observation again clearly indicates alloyed α-CuAl particles, protected by some kind of an oxidation inhibiting shell, which seems to be composed of alumina preferentially. In contrast, the absorption of a nano-Cu reference colloid quickly shifts upon oxidation to 610 nm as the result of CuO_x@Cu core−shell particle formation.[23,32] While these CuO_x@Cu core−shell particles can be reduced in solution by addition of CO, syn-gas, or pure H_2,[33b] the oxidized α-CuAl colloids discussed here showed no change at all upon similar reductive treatment. Preferential Al oxidation and Al_2O_3 surface layer formation is known for single-crystal aluminide thin films of the more electronegative transition metals,[37] with NiAl to yield γ-Al_2O_3@NiAl as a well-studied example.[38]

We believe that the Cu or Cu/Al alloy core is not being substantially oxidized, as long as the Al content is above 15 atom %. Below a level of 15 atom % Al, the Cu component

cannot be effectively passivated by the growth of a dense Al_2O_3 layer and appears to be oxidized as well, resulting in the typical color change from red to green, and the characteristic UV−vis absoption at 604 nm occurs (Figure 6d). The UV−vis spectra of these samples clearly resembled those of pure oxidized Cu@PPO colloids of the core−shell type CuO_x@Cu (Figure 6e). In addition, the ^{27}Al NMR signals for Al_2O_3 were clearly seen in intentionally oxidized $Cu_{1-x}Al_x$ samples, suggesting a surface decorated structure Al_2O_3@$Cu_{1-x}Al_{x-\delta}$ ($0.10 \leq x \leq 0.50$; $\delta < x$). In accordance, powder diffraction diagrams of $Cu_{1-x}Al_x$ colloids ($0.17 \leq x \leq 0.33$), oxidized by treatment with O_2 before precipitation, showed that, in the samples down to 20 atom % Al, Cu(0) is still visible, whereas in the sample with 10 atom % Al, Cu_2O was found in addition to Cu (Figure 4). This points to incomplete oxidation of Cu, most presumably forming a multiphase composite or core−shell particles with a mixed Cu_2O/Al_2O_3 surface structure. That structural damage resulting from oxidation of those α-CuAl alloy particles is also indicated by the line broadening of the remaining fcc Cu reflexes.

Conclusion

Our results suggest $(AlCp^*)_4$ as an exotic but quite interesting precursor to be generally applicable for wet-chemical nanometallurgy of late transition metal aluminides, for example, extending the scope of Chaudret et al.'s work[1] on metal colloids toward classical Hume−Rothery phases. Following the lines outlined above, we already obtained Fe/Al, Co/Al, and Pd/Al materials which we are currently investigating. The Cp* moiety turns out to be an advantageous leaving group being cleanly split off by hydrogenolysis. Important other alloy components, being notoriously difficult to introduce by simple salt reduction, such as Mg, Zn, and Si, may thus as well be applicable via $[MgCp^*_2]$,[39] $[ZnCp^*_2]$,[40] and $[SiCp^*_2]$[41] as precursors. Just to give an inspiring example, we like to cite the unusual molecular $SiAl_{14}$ cluster, $[(Cp^*Al)_6(SiAl_8)]$, being obtained by employing $[SiCp^*_2]$ as the Si source.[42] Consequently, the use of $[ZnCp^*_2]$ instead of $ZnEt_2$ has aided our nanobrass chemistry, and we have now obtained $Cu_{1-x}Zn_x$ colloids of improved purity in comparison with our previous work according to extended X-ray absorption fine structure studies.[23] In addition, we like to emphasize here our related molecular cluster chemistry of $[M_a(ECp^*)_b]$ (M = Fe, Ru, Ni, Pd, Pt; E = Al, Ga, In) which may be of future relevance also in terms of single molecule precursors for alloys or as building blocks for molecularly defined Hume−Rothery type large clusters.[43]

The surface oxidation of the title α-CuAl alloy particles, that is, their redox chemistry, bears interesting perspectives, even beyond the study of Hume−Rothery nanophases and their materials properties as such. For example, oxidized α-CuZn particles, that is, Cu particles decorated with isolated ZnO surface species, may be interesting model catalysts for methanol synthesis from CO/CO_2 and H_2.[5] On the basis of the work discussed above, we are now trying to selectively prepare multiphase $Cu/ZnO/Al_2O_3$ single-particle nanocomposites by controlled corrosion of free-standing ternary Cu/Zn/Al alloy particles, accessible by co-hydrogenolysis of **1** and **2** together with $[ZnCp^*_2]$, to serve as novel *colloidal* congeners for the heterogeneous methanol catalyst.[44] Last but not least, the Fe, Co, Ni, or binary FeCo, FePt, and $CoPt_3$ nanoparticles in the focus of investigations for magnetic properties,[1,45] possibly relevant to novel data storage media and typically synthesized by organometallic wet-chemical methods quite compatible with our example here, may be alloyed with small amounts of Al and then oxidized to yield bimetallic core−shell nanoparticles with the Al_2O_3 shell effectively protecting the magnetic core alloy.

Acknowledgment. The authors thank the German Research Foundation (DFG) for support within the Research Centre 558 "Metal Support Interaction in Heterogeneous Catalysis". Valuable discussions with Prof. Dr. Yuri Grin, Dr. Marc Armbrüster, and Dr. Frank Haarmann (Max-Planck Institute for Chemical Physics of Solids, Dresden) as well as the gift of an authentic $CuAl_2$ reference sample are gratefully acknowledged. We thank Dr. A. Chemseddine, Hahn-Meitner Institute Berlin, for his friendly assistance with HRTEM measurements. The authors are also greatly indebted to Hans-Jochen Hauswald, NMR department of the Ruhr-Universität, Bochum, for ^{1}H and ^{27}Al MAS NMR measurements.

CM052667W

(37) Grabke, H. J. *Mater. Sci. Forum* **1997**, *251−2*, 149.
(38) Ceballos, G.; Song, Z.; Pascual, J. J.; Rust, H.-P.; Conrad, H.; Bäumer, M.; Freund, H.-J. *Chem. Phys. Lett.* **2002**, *359*, 41.
(39) Duff, A. W.; Hitchcock, P. B.; Lappert, M. F.; Taylor, R. G. *J. Organomet. Chem.* **1985**, *293*, 271.
(40) Blom, R.; Boersma, J.; Budzelaar, P. H. M.; Fischer, B.; Haaland, A.; Volden, H. V.; Weidlein, J. *Acta Chem. Scand., Ser. A* **1986**, *40*, 113.
(41) Jutzi, P.; Kanne, D.; Krüger, C. *Angew. Chem., Int. Ed. Engl.* **1986**, *25*, 164.
(42) Purath, A.; Dohmeier, C.; Ecker, A.; Köppe, R.; Krautscheid, H.; Schnöckel, H.; Ahlrichs, R.; Stoermer, C.; Friedrich, J.; Jutzi, P. *J. Am. Chem. Soc.* **2000**, *122*, 6955.
(43) (a) Steinke, T.; Gemel, C.; Cokoja, M.; Winter, M.; Fischer, R. A. *Angew. Chem., Int. Ed.* **2004**, *43*, 2299. (b) Steinke, T.; Gemel, C.; Winter, M.; Fischer, R. A. *Chem.−Eur. J.* **2005**, *11*, 1636. (c) Steinke, T.; Cokoja, M.; Gemel, C.; Kempter, A.; Krapp, A.; Frenking, G.; Zenneck, U.; Fischer, R. A. *Angew. Chem., Int. Ed.* **2005**, *44*, 2943.
(44) (a) Ressler, T.; Kniep, B. L.; Kasatkin, I.; Schlögl, R. *Angew. Chem., Int. Ed.* **2005**, *44*, 4704. (b) Hermes, S.; Schröter, M.-K.; Schmid, R.; Khodeir, L.; Muhler, M.; Tissler, A.; Fischer, R. W.; Fischer, R. A. *Angew. Chem., Int. Ed.* **2005**, *44*, 6237.
(45) (a) Desvaux, C.; Amiens, C.; Fejes, P.; Renaud, P.; Respand, M.; Lecante, P.; Snoeck, E.; Chaudret, B. *Nat. Mater.* **2005**, *4*, 750. (b) Dumestre, F.; Chaudret, B.; Amiens, C.; Respaud, M.; Fejes, P.; Renaud, P.; Zurcher, P. *Angew. Chem., Int. Ed.* **2003**, *42*, 5213. (c) Cordente, N.; Respaud, M.; Senocq, F.; Casanove, M.-J.; Amiens, C.; Chaudret, B. *Nano Lett.* **2001**, *1*, 565. (d) Sun, S.; Murray, C. B.; Weller, D.; Folks, L.; Moser, A. *Science* **2000**, *287*, 1989. (e) Shevchenko, E.; Talapin, D. V.; Schnablegger, H.; Kornowski, A.; Festin, Ö.; Svedlindh, P.; Haase, M.; Weller, H. *J. Am. Chem. Soc.* **2003**, *125*, 9090.